JME
Journal of Mining & Environment,
Vol.9, No.1, 2018, 41-52.
DOI: 10.22044/jme.2017.5522.1364

Hydrothermal alterations mapping using Quickbird and Landsat-8 data, a case study from Babbiduyeh, Kerman province, Iran

H. Aryanmehr, M. Hosseinjani Zadeh*, M. Honarmand and F. Naseri

Department of Ecology, Institute of Science and High Technology and Environmental Sciences, Graduate University of Advanced Technology, Kerman, Iran

Received 14 March 2017; received in revised form 7 October 2017; accepted 16 October 2017
**Corresponding author: mh.hosseinjani@gmail.com (M. Hosseinjani Zadeh).*

Abstract
In this work, we focus on investigating the Quickbird and Landsat-8 datasets for mapping hydrothermal and gossans alterations in reconnaissance porphyry copper mineralization in the Babbiduyeh area. This area is situated in the Central Iranian Volcano-sedimentary Complex, where large copper deposits like Sarcheshmeh as well as numerous occurrences of copper exist. The alteration zones are discriminated by implementation of band ratio and principal component analysis on the Quickbird and Landsat-8 datasets. The image processing results are evaluated by field surveys, X-ray diffraction (XRD), microscopic thin section, and spectroscopic studies of field samples as well as the 1:100000 Sarduiyeh and 1:5000 Babbiduyeh geological maps. In addition, the spectral characterizations of the samples are analyzed by visual inspection, and the PIMAView, SAMS, and ViewSpecpro software programs. The combined spectroscopic measurements, XRD analyses, and petrographic studies revealed mineral assemblages typical of the phyllic, phyllic-supergen, propylitic, argillic, and gossan alterations. The results obtained from image processing and analysis of field samples illustrated examples of effects of iron oxides and hydroxides on the surface of phyllic and argillic alterations. Hence, it can be concluded that the areas discriminated in Quickbird as gossans correspond to the phyllic and argillic alteration areas.

Keywords: *Band Ratio, Hydrothermal Alteration, Landsat-8, Principal Component Analysis, Quickbird.*

1. Introduction

Central Iranian Cenozoic Magmatic Belt (CICMB) has a significant potential for porphyry copper mineralization. Many researchers have applied the remote sensing and geographic information system techniques on CICMB for mapping hydrothermal alteration, especially in porphyry copper deposits [1-6].

Porphyry copper deposits are associated with the hydrothermal alteration zones such as phyllic, argillic, potassic, and propylitic. These zones may be affected by leaching and supergene alteration over porphyry copper deposits, and produce an oxide zone with hydroxide minerals including dissolution boxes, named gossan. These alteration zones contain specific minerals such as muscovite, kaolinite, biotite, alunite, chlorite, hematite, and jarosite, which show diagnostic absorption features in different parts of the electromagnetic spectrum, especially in the VNIR and SWIR region due to the chemical and mineralogical variations [7-10]. This characteristic offers a potential for mineral identification (especially, gold and copper) through remote sensing studies. The ability of remote sensing in discrimination of porphyry copper alterations using various sensors such as ASTER, TM, ETM^+, and hyperion has been reported in many studies [1- 5, 9-17]. However, relatively little publications are available for mapping alteration minerals using sensors such as OLI in Landsat-8 and Quickbird (a high spatial resolution sensor). Therefore, much more works should be carried out using these sensors. Quickbird that contains high spatial resolutions of

2.44 m and 0.61 m with four spectral bands in the VNIR region (covering the 0.45–0.90 μm range) may be suitable for discrimination of gossans (Table 1). The Quickbird dataset has been used in geological mapping and hazard assessing in the recent years [18-22]. Girouard et al. (2004) have compare the results between Quickbird and Landsat TM as high and medium spatial resolution sensors, respectively, to validate the Spectral Angle Mapper (SAM) algorithm for geological mapping in Central Jebilet Morocco [19]. Aydal et al. (2008) have used GIS and different processing methods including band combination, principal component analysis, crosta technique, band rationing, decorrelation stretching, and various filtering techniques on the ETM+ and Quickbird data to determine unknown ore deposits/enrichments in Hinzar Mountain in Turkey [20]. Liu et al. (2013) have used ETM+ and Quickbird for mapping lithological units, small intrusions, and alteration zones to target mineral resources in the Xiemisitai area, west Junggar, Xinjiang, China [21]. Mishra et al. (2014) have used the ASTER and Quickbird data to identify the chloritic and phyllic alteration zones and gossans related to gold mineralization in North Sudan [22].

Landsat-8 satellite is a new product from NASA under Landsat open source series, which was launched in February 2013. It carries two sensors including the Operational Land Imager (OLI) and Thermal Infrared Sensor (TIRS) along with three new bands: a deep blue band for coastal/aerosol studies, a shortwave IR band for cirrus detection, and a quality assessment band. The Landsat-8 data can detect the alterations and iron oxyhydroxide minerals due to the absorption and reflectance characteristics of these minerals through the OLI (Operational Land Imager) sensor with two spectral bands in the short-wave infrared (SWIR) and 5 bands in the visible near infrared (VNIR) (Table 2). Since the advent of Landsat-8, many researchers have used the landat-8 data in their studies [24-29]. Fotovat Roudsari and Solgi (2014) have used the Landsat-8 and ASTER data for identification of altered tuff and supergene zone to prospect polymetallic mineralization in Ferdows area, Iran [30]. Ahmed and Beiranvand Pour (2014) have used the conventional image processing methods such as color composite, principle component analysis, band ratio, and minimum noise fraction on the Landsat-8 data to find and map the lithological units and alteration zones in a gold mining area in NE Sudan [28]. Khalid et al. (2014) have carried out general prospecting in the gold deposit near Khartoum, Sudan, and searched for possible mineral deposits through an integrated analysis of the satellite gravity and Landsat 8 OLI data [31]. Beiranvand Pour and Hashim (2014) have studied the applicability of Landsat-8 for mapping hydrothermal alteration areas and lithological units associated with porphyry copper exploration in Sarcheshmeh Copper Mine, SE Iran (29). Mwaniki et al. (2015) have compared Landsat-8 and 7 for geological mapping and visualizing lineaments in the central region of Kenya [32]. The mentioned studies revealed the importance of Landsat-8 and Quickbird in geological studies and mineral mapping.

The main purpose of this work was to investigate the Quickbird and Landsat-8 datasets to map hydrothermal alterations and gossan in reconnaissance porphyry copper mineralization in the Babbiduyeh area. The other purpose was to validate and find the relationship between these two satellite images with field studies and sample analysis such as X-ray diffraction (XRD) analyzes, microscopic thin sections, and spectroscopy studies.

Table 1. Characteristics of Quickbird sensor [23].

Launch Date	October 18, 2001
Orbit Altitude	450 Km
Swath Width	16.5 Km at nadir
Digitization	11 bits
Resolution	Pan: 61 cm (nadir) to 72 cm (25° off-nadir) MS: 2.44 m (nadir) to 2.88 m (25° off-nadir)
Image Bands	Pan: 450-900 nm Blue: 450-520 nm Green: 520-600 nm Red: 630-690 nm Near IR: 760-900 nm

Table 2. Characterizations of Landsat-8 sensor [33].

Band Name	Wavelength	Spatial Resolution
Coastal/Aerosol	0.433-0.453 µm	30 m
Blue	0.450-0.515 µm	30 m
Green	0.525-0.600 µm	30 m
Red	0.630-0.680 µm	30 m
Near IR	0.845-0.885 µm	30 m
Shortwave IR	1.560-1.660 µm	30 m
Shortwave IR	2.100-2.300 µm	30 m
Panchromatic	0.500-0.680 µm	15 m
Cirrus	1.360-1.390 µm	30 m
Thermal IR	10.60-11.19 µm	100 m
Thermal IR	11.50-12.51 µm	100 m

2. Location and geological settings of studied area

The Babbiduiyeh area is located in the southern part of the Central Iranian Volcano-Sedimentary Complex (Uromiyeh-Dokhtar Belt) in the Kerman Cenozoic Magmatic Arc (KCMA) or Dehaj-Sarduiyeh copper belt, SE of Kerman province (Figure 1). The studied area is located in a mountainous semi-arid environment with low vegetation, in which the altitude varies between 1600 and 4391 m above the sea level, and therefore, it is ideal for remote sensing studies. CICMB is considered to have a suitable economic potential regarding copper mineralization, and it is analog to the important porphyry copper belts of the world such as Andean volcanic belt [34, 35]. Numerous occurrences of copper mineralization including the great deposit of Sarcheshmeh have been discovered at this belt.

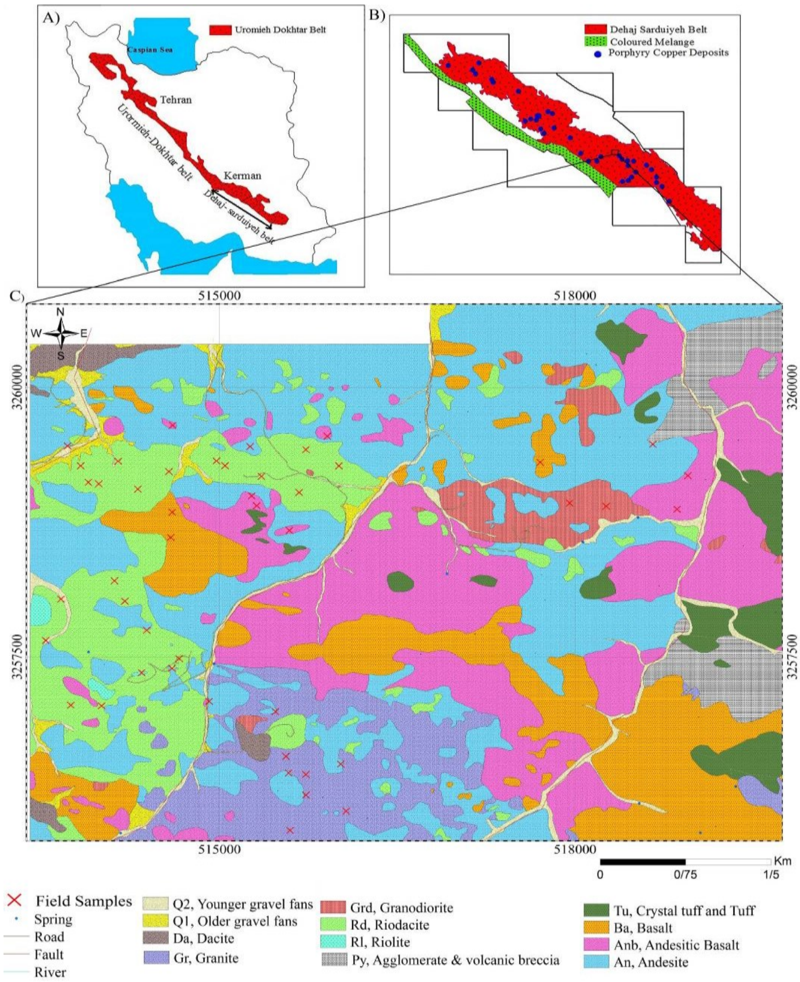

Figure 1. A) Geographical location of studied area in Iran B) in Kerman Cenozoic Magmatic Arc (Dehaj-Sarduiyeh belt) [29] C) 1:5000 Geological map of Babbiduyeh [36].

Copper mineralization in the Babbiduyeh area is related to the Oligomiocene granodioritic intrusions, which penetrated in the volcano-sedimentary rocks of Eocene. According to the geological map of the Babbiduyeh area, the dominant lithology is igneous rocks. Dacites, riodacites, rhyolite, granite, and granodiorites in the area are related to Cenozoic Era, Neogen period. Other existent lithological units in the studied area involve andesite, andesite- basalt, and basalt with pyroclastic. In addition, conglomerate, trace sandstone, gravel, and recent age alluvium spread in the northern part of the region (Figure 1). Mineralization, which mostly occurs as porphyry copper, focuses at the central and southern part of Babbiduyed in sub-volcanic stock. Porphyry copper in Babbiduyeh is associated with the hydrothermal alteration zones such as phyllic, argillic, potassic, and propylitic. These zones were affected by leaching and supergene alteration, and produced an oxide zone with oxide and hydroxide minerals including dissolution boxes, named gossans (Figure 2).

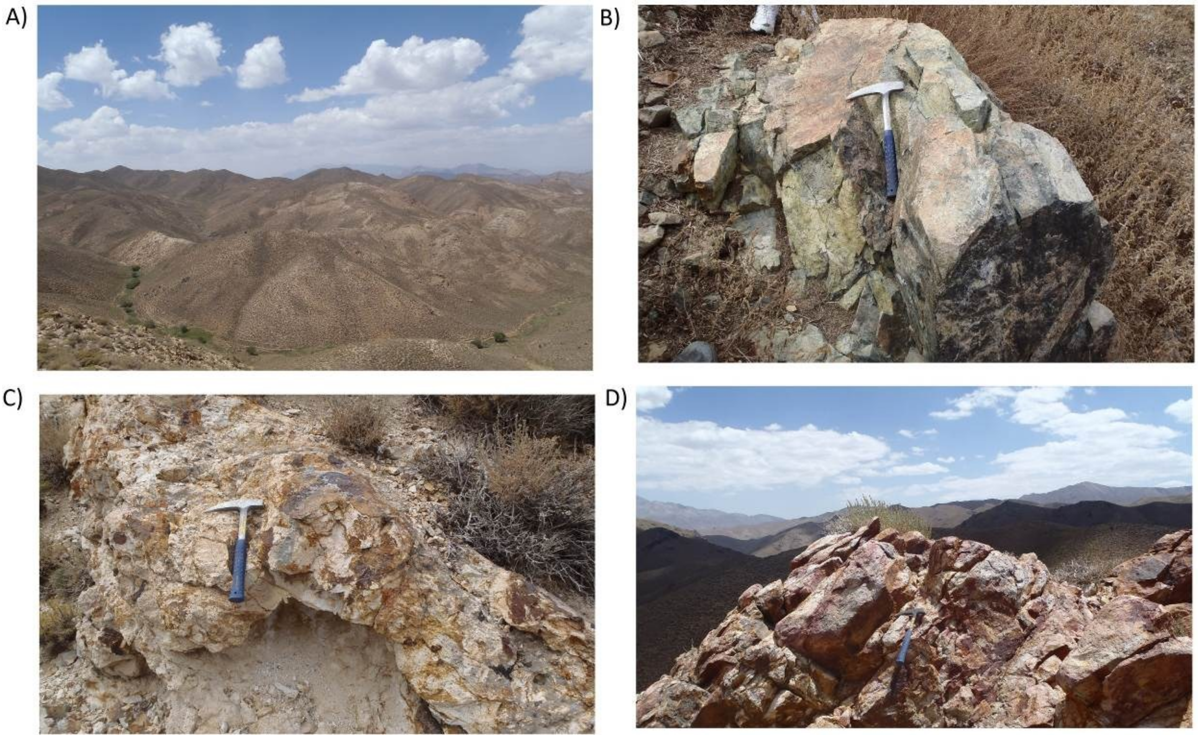

Figure 2. Some photos taken during field study. A) General view of studied area B) Propyllitic alteration C) Argillic alteration D) Phyllic alteration. In photos C and D, iron oxide minerals can be observed at surface of phyllic and argillic alterations.

3. Methods

The Quickbird and Landsat-8 images were used in this research work for mapping the alteration minerals. DigitalGlobe's QuickBird image data was typically distributed in a relative radiance. Pre-processing was implemented on the data in order to remove noise and acquire surface reflectance. The QuickBird radiance calibration utility from ENVI 5.1 software was used to convert the relative radiance into the absolute radiance in units of [(μW)/(cm^2*nm*sr)]. The calibration was performed using the calibration factors in the QuickBird metadata file (the absCalFactor value in the.imd file). The units were converted from [W/(m^2*sr)] into [(μW)/(cm^2*nm*sr)] using nominal band pass widths of bands blue (68 nm), green (99 nm), red (71 nm), and NIR (114 nm) [37]. The IARR pre-processing was applied on the absolute radiance data to normalize the image and convert data to relative reflectance. The geometric correction was also implemented using topographic maps and drainage network of the studied area. The pre-processing of Landsat-8 includes dark subtract correction to reduce the atmospheric effects. The downloaded Landsat-8 data was pre-georeferenced to UTM zone 40-North projection. While pre-processing was applied to the data, the alteration minerals were enhanced by implementation of image-based algorithm including band ratioing and principal component analysis (PCA). Since Landsat-8 and

Quickbird are multi-spectral sensors containing few bands, it is better to use image-based algorithms instead of spectral-based ones such as linear spectral unmixing (LSU), matched filtering (MF), and mixture-tuned matched filtering (MTMF). In order to acquire information about alteration minerals and mineralogical characteristics at the Babbiduiyeh area, a field reconnaissance was carried out, and 50 samples were collected through a systematic sampling from fresh and representative hydrothermally altered rocks using a Global Positioning System (GPS) (Figure 1C). The mineralogy of samples was studied using XRD, spectroscopic studies, and transmitted reflected light microscopy. The ENVI 5.1, ArcGIS 10.3, PimaView, ViewSpecpro, and SAMS softwares were used for pre-processing and processing the satellite images and recognizing the field spectra.

4. Results and discussions

4.1. Mineralogical studies

The mineralogy of samples was studied using XRD, transmitted/reflected light microscopy, and spectroscopic studies. According to the major, minor, and trace phases of twenty one XRD analyses from field samples, four alteration zones including phyllic (13 samples), albitization (3 samples), silicic-phyllic (3 samples), and gossan (2 samples) were identified.

Spectra of the samples were measured using an analytical spectral device (ASD) field-portable FieldSpec3® spectro-radiometer, which measures reflectance spectrum across a spectral range of 325–2500 nm with 10 nm individual band width. Multiple spectra were acquired from both fresh and weathered facets of the samples taking into account that they are mixtures of different minerals, and less abundant minerals may not be observed in one single measurement [7]. Approximately 138 spectra were measured from 50 samples, and were analyzed to characterize the hydrothermal and supergene alteration minerals using the Pima view V3.1 and ENVI 5.1 softwares. Furthermore, an automated mineral identification was implemented by creating a reference spectral library through PIMA View v3.1 to simplify and speed-up the process of spectral analysis. Since significant minerals such as quartz, feldspar, pyrite, and chalcopyrite do not have characteristic absorption features in the VNIR-SWIR region, extraction of mineral information was focused on the main hydrothermal alteration products, which could be recognized by spectroscopic analysis. The identified minerals include muscovite, illite, montmorillonite, goethite, hematite, Jarosite, chlorite, and epidote (Figure 3). According to the particular characteristics of spectra in VNIR-SWIR regions, phyllic-oxide, phyllic, propylitic, argillic, and oxide alteration (gossan) zones could be distinguished.

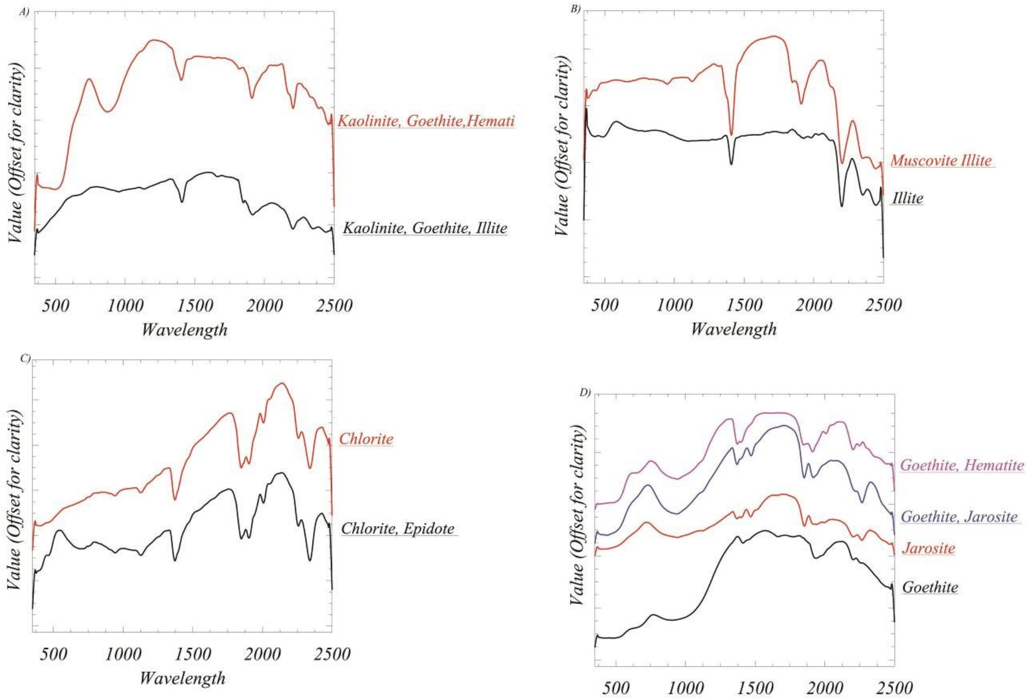

Figure 3. Different types of alteration minerals identified by spectroscopic studies A) argillic B) phyllic C) propylitic D) gossan.

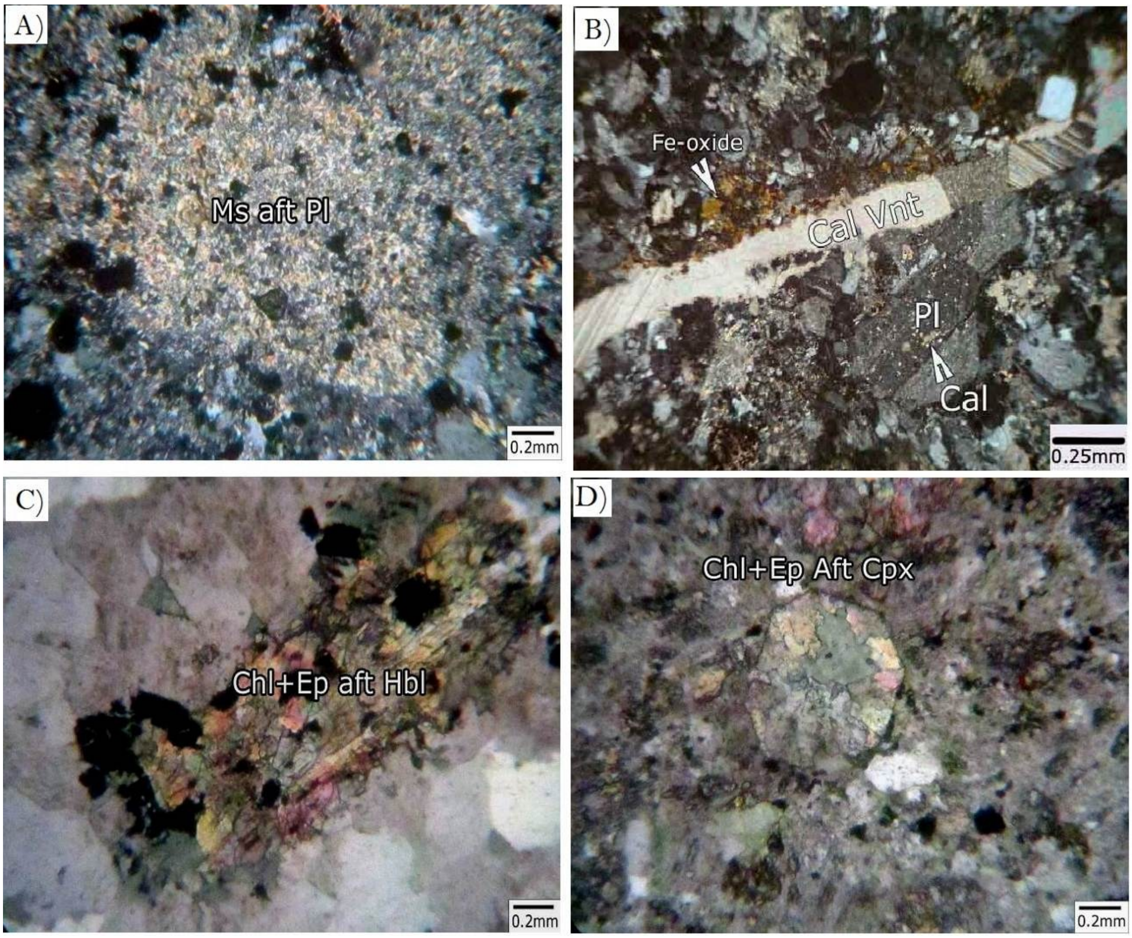

Figure 4. Microscopic thin sections of some samples observed in crossed polarized light A) Plagioclase phenocrysts are pervasively replaced by muscovites B) Veinlet of calcite with iron oxide C) Hornblane phenocrysts are replaced by chlorite and epidote D) Clinopyroxen phenocrysts are replaced by chlorite and epidote.

Microscopic examination revealed that most of the samples essentially consisted of secondary minerals including sericite, kaolinite, epidote, chlorite, calcite, jarosite, goethite, and hematite formed at a later time through processes such as hydrothermal alteration and weathering. Furthermore, quartz, plagioclase, alkali feldspar, amphibolite, pyroxene, chalcopyrite, pyrite, titanum oxide, and magnetite are also observed in the samples (Figure 4). However, since the clay minerals were composed of very fine-grained particles in the majority of samples, it was very difficult to identify them correctly under microscopic studies.

4.2. Processing satellite images

4.2.1. Band ratio

Band ratio is a multi-spectral image processing method that divides the digital number of one band to another one. Same surface minerals due to trend, topographic slope, shadow or seasonal changes in intensity and brightness angle of sun light indicate different radiance values [38]. These distorting effects cause errors in interpretation of supervisor and have misleading results. The band ratio process could minimize these environmental effects. Spectral band rationing enhances compositional information, while suppressing other types of information about earth's surface. This method is very useful for highlighting certain features or materials that cannot be seen in the raw bands. Band ratio transformation is useful for a qualitative detection of hydrothermal alteration minerals [39, 40].

The argillic and phyllic zones are characterized by muscovite/illite and kaolinite. These minerals exhibit an intense Al-OH spectral absorption and reflectance features typically centered at 2.20 and 1.65 μm, respectively. According to the resample spectra of these minerals into Quickbird and Landsat-8, these absorption and reflectance features coincided with the bands 7 and 6 of Landsat-8, respectively (Figure 5). However, due to the lack of adequate bands in this region at Quickbird, it is not possible to identify clay minerals through this sensor. As a result, the band ratio of 6/7 of Landsat-8 was used to enhance the kaolinite, muscovite, and clay minerals. The discriminated areas were enhanced as bright pixels and were corresponded to the results obtained from the XRD and spectroscopic studies (Figures 5B and 5C).

The VNIR bands contain chief information about the absorption features related to transition metals (e.g. Fe^{2+}, Fe^{3+}) within the oxide zone including jarosite, goethite, and hematite. These minerals exhibit prominent spectral absorption and reflectance features in the blue and red regions, respectively (near 0.44 and 0.67 µm), which coincide with band 2 of Landsat-8 and band 1 of Quickbird (Table 3, Figure 5). Therefore, it is possible to identify oxide minerals through Landsat-8 and Quickbird by applying the image-based techniques such as band ratio. The ratio 4/2 (Figures 6E and 6F) of Landsat-8 is useful for enhancing iron oxides because it has absorption in the blue and high reflectance in the red region. VNIR bands of Landsat-8 and Quickbird are nearly equivalent (Table 3), so that bands 4 and 2 of Landsat-8 are equal to bands 3 and 1 of Quickbird, respectively. Therefore, the band ratios 4/2 and 3/1 for Landsa-8 and Quickbird, respectively, are used for identification of the oxide zone or gossan. Comparison of the Quickbird and Landsat-8 results obtained from these band ratios revealed that the discriminated areas coincided (Figures 6E, 6F, 6H, and 6I). A higher spectral resolution in Landsat-8 facilitates the discrimination of more features such as clay and oxide minerals. Although it is not possible to discriminate clay minerals in Quickbird due to the lack of SWIR bands, a higher spatial resolution of Quickbird permits an accurate location of the features.

4.3. Principle component analysis (PCA)

PCA is a powerful statistical technique used to suppress irradiance effects and reduce the data redundancy by transforming the original data onto new principal component axes. Therefore, this technique produces an uncorrelated image, which has a much higher contrast than the original bands. PCA can be applied to the multivariate datasets such as multi-spectral remote sensing images, with the purpose of extracting specific spectral responses, as in the case of hydrothermal alteration minerals. This technique relies on establishing the relationship between the spectral responses of target materials such as alteration minerals. In this algorithm, numeric values could be extracted from the eigenvector matrix and used to calculate the principal component (PC) images. Using this relationship, it is possible to determine which PCs contain the spectral information of the target minerals by investigation of digital numbers (DNs) of pixels or eigenvector matrix containing high (bright) or low (dark) values [41].

The result of this method was uncorrelated PC bands equal to the number of bands. In order to determine which image contains information related to the spectral signatures of specific alteration and oxide minerals, eigenvector loadings in each PC image were examined. The PC image with moderate-to-high eigenvector loadings for diagnostic absorptive and reflective bands of the argillic-phyllic and oxide/hydroxide minerals were considered as the representative image for these minerals.

According to the spectral characteristics of iron oxide/hydroxide minerals (Figure 5A), bands 3 and 1 of Quicbird and bands 4 and 2 of Landsat-8 that correspond to the reflective and absorptive bands, can discriminate areas rich in these minerals. In addition, the reflective and absorptive bands 6 and 7 of Landsat-8 are suitable for detecting alteration minerals such as sericite, kaolinite, chlorite, and epidote. If the loading of the absorptive and reflective bands are negative and positive, respectively, in sign, the target area is shown by bright pixels; conversely, if the loading of the absorptive and reflective bands are positive and negative, the area is shown by dark pixels.

Tables 4 and 5 list the eigenvector matrix for the PCA results on the Quickbird and Landsat-8 bands. According to the eigenvector loading of Landsat-8, PC4 is appropriate for discrimination of alteration minerals as bright pixels due to the high positive loading in band 6 and high negative loading in band 7 (Figures 7B and 7C, and Table 4). PC5 for Landsat-8 could highlight areas of oxide/hydroxide minerals because it contains higher negative loadings for bands 1 and 2 and positive loading for band 4 (Table 4). The PC images are shown in Figures 7E and 7F.

Investigation of the eigenvector loadings for Quickbird show that PC3 contains high loading for bands 1 and 3 in positive and negative signs, which is ideal for discrimination of oxide/hydroxide minerals or gossan areas as dark pixels (Table 5). In order to show the areas containing these minerals as bright pixels, the inverse of PC3 was obtained (Figures 7H and 7I).

Table 3. Comparison of VNIR bands of Quickbird and Landsat-8.

VNIR bands of Landsat-8	VNIR bands of Quickbird image
B2: 450-515 nm	B1: 450-520 nm
B3: 525-600 nm	B2: 520-600 nm
B4: 630-680 nm	B3: 630-690 nm
B5: 845-885 nm	B4: 760-900 nm

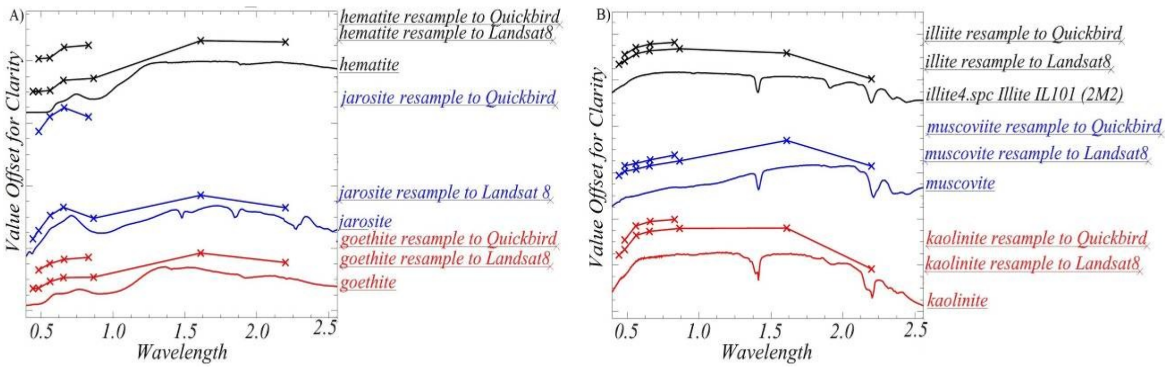

Figure 5. Spectral plots of some minerals extracted from USGS spectral library and resample to band centers of Landsat-8 and Quickbird. A) Some iron oxide/hydroxide/sulfate minerals B) some clay minerals.

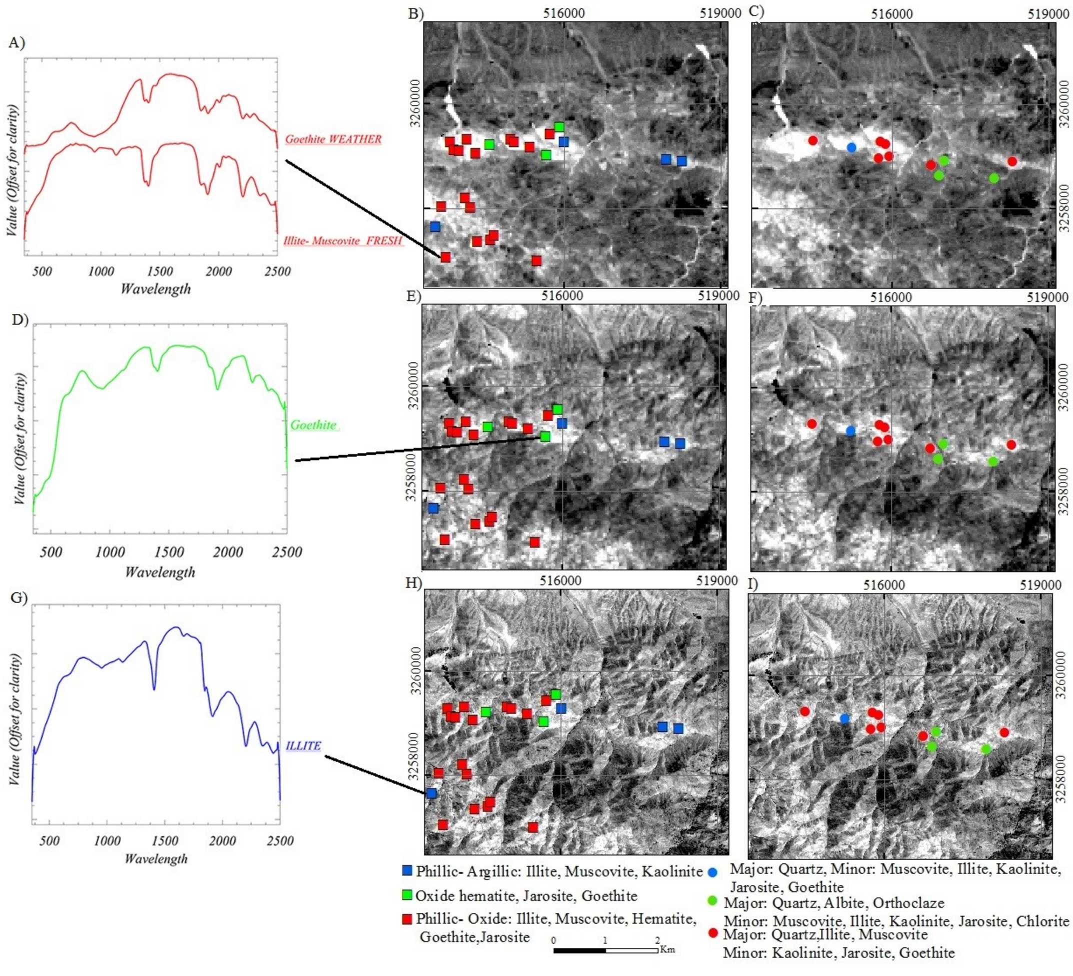

Figure 6. A) ASD spectral plot of a sample containing illite (fresh facet) and goethite (weathered facet) and its location on image B C) Band ratio 6/7 of Landsat-8 compared with spectroscopic studies and XRD, respectively, ASD spectral plot of a sample contains goethite and its location on image E F) Band ratio 4/2 of Landsat-8 compared with spectroscopic studies and XRD, respectively G) ASD spectral plot of a sample containing illite and its location on image H I) Band ratio 3/1 of Quickbird compared with spectroscopic studies and XRD, respectively.

Table 4. Eigenvector matrix for PCA results of Landsat-8.

	Band 1	Band 2	Band 3	Band 4	Band 5	Band 6	Band 7
PC1	0.105	0.138	0.231	0.337	0.459	0.609	0.470
PC2	-0.745	-0.103	-0.117	-0.214	0.865	-0.148	-0.393
PC3	-0.345	-0.393	-0.410	-0.533	-0.068	0.448	0.262
PC4	-0.084	-0.075	0.110	0.189	-0.189	0.598	-0.739
PC5	-0.403	-0.491	-0.264	0.695	0.0424	-0.190	0.070
PC6	0.490	0.244	-0.806	0.186	-0.001	0.111	-0.062
PC7	-0.675	0.713	-0.182	0.045	0.008	0.002	-0.012

Table 5. Eigenvector matrix for PCA results of Quickbird.

	Band 1	Band 2	Band 3	Band 4
PC1	0.366	0.475	0.581	0.550
PC2	0.428	0.345	0.213	-0.808
PC3	0.656	0.123	-0.714	0.211
PC4	0.503	0.800	-0.327	-0.011

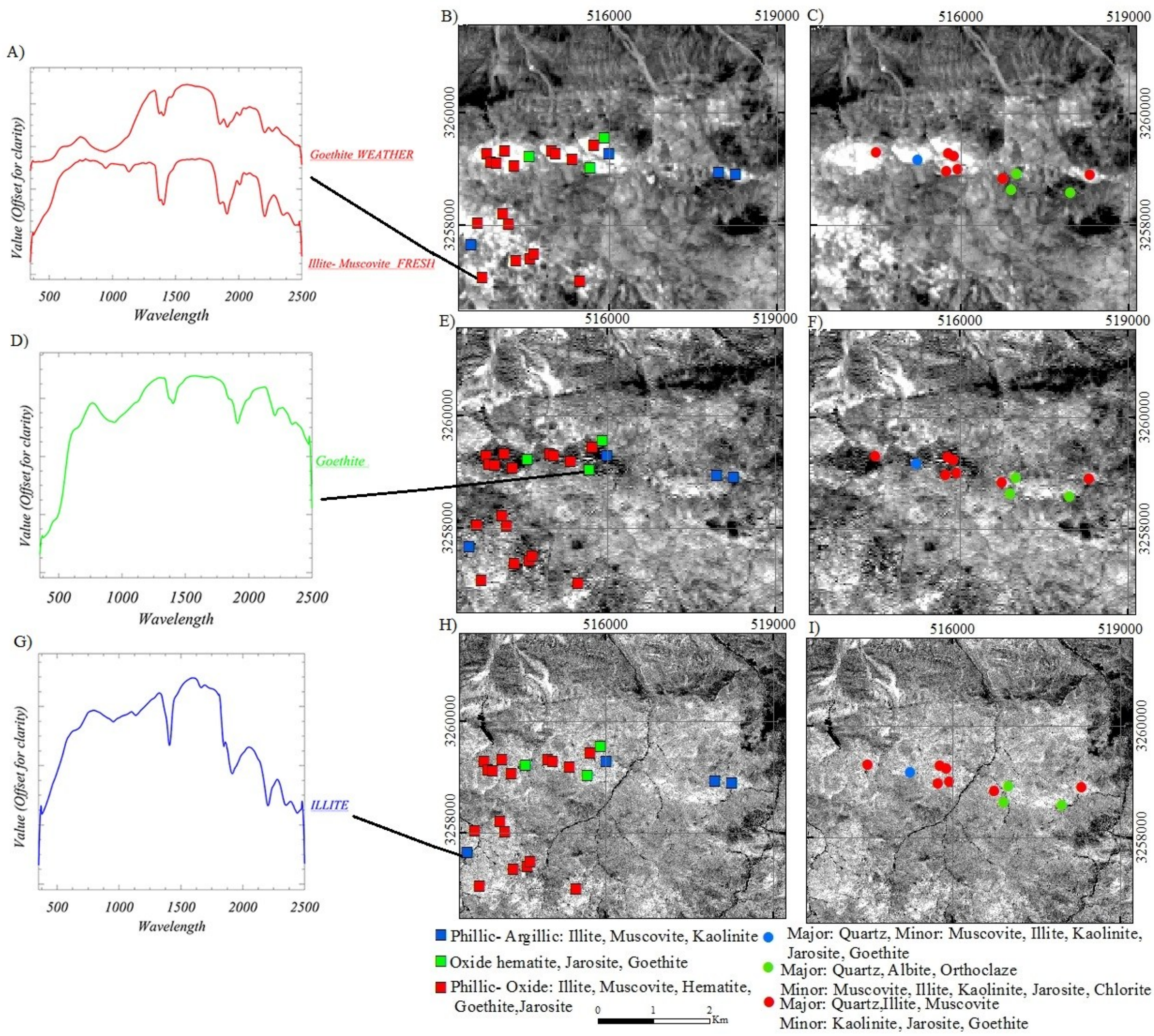

Figure 7. A) ASD spectral plot for a sample containing illite (fresh facet) and goethite (weathered facet) and its location on image B C) PC4 of Landsat-8 compared with spectroscopic studies and XRD, respectively D) ASD spectral plot for a sample containing goethite and its location on image E F) PC5 of Landsat-8 compared with spectroscopic studies and XRD, respectively G) ASD spectral plot of a sample containing illite and its location on image H I) Inverse PC3 of Quickbird compared with spectroscopic studies and XRD, respectively.

5. Accuracy assessment

The discriminated altered areas were verified by field surveys, geological maps of the studied area, and laboratory analyses such as XRD, spectroscopic studies, and transmitted and reflected light microscopy. There is a distinct link between image processing results and analysis data in the Babbiduyeh area. The results of spectroscopic studies, which revealed the existence of goethite, hematite, muscovite, and illite in the samples, correspond to the band ratio and PCA results as well (Figures 6 and 7). According to the spectroscopic studies by ASD fieldSpec[3], illite, muscovite, and kaolinite were observed in the argillic-phillic zones and hematite, jarosite, goetite in the oxide zones. In some samples, Jarosite, goethite, and hematite were discriminated in the weatherd surface, while illite and muscovite were observed in fresh surface (Figures 6 and 7 (A, D, and G)). These samples are normally from the supergen zones, where oxide minerals lie on phyllic and argillic alteration. The XRD results show the existance of quartz, muscovite, illite, albite, and orthoclase in the major phase, and goetite and jarosite in the minor phase (Figures 6 and 7 (C, F, and I)). According to the geological map of the studied area, the discriminated areas coincided with the riodacite, granodiorite, and granite rocks. Thin sections of these rocks showed existance of Fe-oxide, chalcophyrite, pyrite, and titanium oxide.

6. Conclusions

In this research work, the alteration zones were mapped by applying the image processing methods such as band ratioing and PCA on Quickbird and Lansat-8. The results obtained were checked through field investigations so that the locations of ground control and sampling points were designed based on the enhanced alteration from image processing. Principal component analysis and band ratioing on Landsat-8 showed a good capability in highlighting the distribution of alteration and oxide-hydroxide mineral assemblages present in the alteration zones. Although the Quickbird data does not contain the SWIR band and could not discriminate alteration minerals, sufficient bands in VNIR can be used in mapping the distribution of iron oxide/hydroxide minerals. There is a general agreement between the results obtained from ASD and XRD analyses and petrographic studies. The combined spectroscopic measurements, XRD analysis, and petrographic studies revealed mineral assemblages typical of phyllic, phyllic-supergen, propylitic, argillic, and oxide alteration (gossan). Analyses of field samples including observations of thin sections, XRD analysis, and spectral measurements revealed that phyllic was most intensive from other hydrothermal alterations in the Babbiduyeh area. Since this type of alteration is usually directly associated with areas of copper mineralization, discrimination of phyllic- argillic alteration associated with oxide minerals could be beneficial in discrimination of PCD. In general, image processing of Quickbird, Landsat-8, and field samples revealed the effect of gossans on hydrothermal alteration zones, which could be useful in reconnaissance studies for porphyry copper identification.

References

[1]. Hosseinjani Zadeh, M. and Tangestani, M.H. (2011). Mapping alteration minerals using sub-pixel unmixing of ASTER data in the Sarduiyeh area, SE Kerman, Iran. International Journal of Digital Earth. 4 (6): 487-504.

[2]. Honarmand, M., Ranjbar, H. and Shahabpour, J. (2012). Application of Principal Component Analysis and Spectral Angle Mapper in the Mapping of Hydrothermal Alteration in the Jebal–Barez Area, Southeastern Iran. Resource Geology. 62: 119-39.

[3]. Khaleghi, M., Ranjbar, H., Shahabpour, J. and Honarmand, M. (2014). Spectral angle mapping, spectral information divergence, and principal component analysis of the ASTER SWIR data for exploration of porphyry copper mineralization in the Sarduiyeh area, Kerman province, Iran. Applied Geomatics. 6 (1): 49-58.

[4]. Shahriari, H., Honarmand, M. and Ranjbar, H. (2015). Comparison of multi-temporal ASTER images for hydrothermal alteration mapping using a fractal-aided SAM method. International Journal of Remote Sensing. 36 (5): 1271-1289.

[5]. Tayebi, M.H. and Tangestani, M.H. (2015). Sub pixel mapping of alteration minerals using SOM neural network model and hyperion data. Earth Science Informatics. 8 (2): 279-291.

[6]. Hosseinjani Zadeh, M. and Honarmand, M. (2017). A remote sensing-based discrimination of high- and low-potential mineralization for porphyry copper deposits; a case study from Dehaj-Sarduiyeh copper belt, SE Iran. European Journal of Remote Sensing. 50 (1): 332-342.

[7]. Hosseinjani Zadeh, M., Tangestani, M.H., Velasco Roldan, F. and Yusta, I. (2014). Spectral characteristics of minerals in alteration zones associated with porphyry copper deposits in the middle part of Kerman

copper belt, SE Iran. Ore Geology Reviews. 62: 191-198.

[8]. Lowell, J.D. and Guilbert, J.M. (1970). Lateral and vertical alteration-mineralization zoning in porphyry ore deposits. Economic Geology. 65: 373-408.

[9]. Kruse, F.A., Boardman, J.W. and Huntigton, J.F. (2003). Comparison of airborne hyperspectral data and EO-1 Hyperion for mineral mapping. IEEE Transactions on Geoscience and Remote Sensing. 41 (6): 1388-1400.

[10]. Mars, J.C. and Rowan, L.C. (2010). Spectral assessment of new ASTER SWIR surface reflectance data products for spectroscopic mapping of rocks and minerals. Remote Sensing of Environment. 114 (9): 2011-2025.

[11]. Galvao, L.S., Filho R.A. and Vitorello, C. (2005). Spectral discrimination of hydrothermal altered materials using ASTER Short wave infrared bands: Evalation in a tropical Savannah Environment. International Journal of Applied Earth Observation and Geoinformation. 7: 107-114.

[12]. Qiu, F., Abdelsalam, M. and Thakka, P. (2006). Spectral analysis of ASTER data covering part of the Neoproterozoic Allaqi-Heiani suture, Southern Egypt. Journal of African Earth Sciences. 44 (2): 169-180.

[13]. Hosseinjani Zadeh, M., Tangestani, M.H., Velasco Roldan, F. and Yusta, I. (2014). Sub-pixel mineral mapping of a porphyry copper belt using EO-1 Hyperion data. Advances in Space Research. 53 (3): 440-451.

[14]. Amer, R., Kusky, T. and Mezayen, A.E. (2012). Remote sensing detection of gold related alteration zones in Um Rus area, Central Eastern Desert of Egypt. Advances in Space Research. 49 (1): 121-134.

[15]. Croft, H., Kuhn, N.J. and Anderson, K. (2012). On the use of remote sensing techniques for monitoring spatio-temporal soil organic carbon dynamics in agricultural systems. Catena. 94: 64-74.

[16]. Mohebi, A., Mirnejad, H., Lentz, D., Behzadi, M., Dolati, A., Kani, A. and Taghizadeh, H. (2015). Controls on porphyry Cu mineralization around Hanza Mountain, south-east of Iran: An analysis of structural evolution from remote sensing, geophysical, geochemical and geological data. Ore Geology Reviews. 69: 187-198.

[17]. Zhang, X. and Li, P. (2014). Lithological mapping from hyperspectral data by improved use of spectral angle mapper. International Journal of Applied Earth Observation and Geoinformation. 31: 95-109.

[18]. Carter, G., Kelly, L., Gabriel, B., Chery, L., Dan, H., David, M., Danielle, F., Tracy, H. and Jerry, G. (2009). Remote Sensing and Mapping of Tamarisk along the Colorado River, USA: A Comparative Use of Summer-Acquired Hyperion, Thematic Mapper and QuickBird Data. Remote Sensing. 1 (3): 318 -329.

[19]. Girouard, G., Bannari, A., El Harti, A. and Desrochers, A. (2004). Validated Spectral Angle Mapper Algorithm for Geological Mapping: Comparative Study between Quickbird and Landsat-TM, in XXth ISPRS Congress, Technical Commission IV Orhan. Altan, Editor. Istanbul. Turkey. pp. 599-604.

[20]. Aydal, D., Gülhan, A., Uslu, A. and Demirkan, A. (2008). Determination of the ore enrichments in Hinzar mountain (Turkey- Kayseri- AkkiŞla) by using Landsat- 7 ETM$^+$ and Quickbird data. Third International Conference on the Geology of the Tethys, Aswan. pp. 227-232.

[21]. Liu, L., Zhou, J., Jiang, D., Zhuang, D., Mansaray, L.R. and Zhang, B. (2013). Targeting Mineral Resources with Remote Sensing and Field Data in the Xiemisitai Area, West Junggar, Xinjiang, China. Remote Sensing. 5: 3156-3171.

[22]. Mishra, B.K., Rao, N.S., Rautray, S. and Pattanayak, S. (2014). An Integrated Geoscientific Approach to Define Zones of Gold Mineralization- A Case Study in North Sudan. Open Journal of Geology. 4: 190-197.

[23]. DigitalGlobe, QuickBird Imagery Products., S. Revision 4.7.1. 1601 Dry Creek Drive, Longmont, Colorado 80503, Editor. 2006.

[24]. Ke, Y., Imb, J., Lee, J., Gong, H. and Ryu, Y. (2015). Characteristics of Landsat 8 OLI- derived NDVI by comparison with multiple satellite sensors and in-situ observations. Remote Sensing of Environment. 164: 298-313.

[25]. Roy, D.P., Kovalsky, V., Zhang, H.K., Vermote, E.F., Yan, L., Kumar S.S. and Egorov A. (2016). Characterization of Landsat-7 to Landsat-8 reflective wavelength and normalized difference vegetation index continuity. Remote Sensing of Environment. 185: 57-70.

[26]. Storey, J., Choate, M. and Lee, K. (2014). Landsat 8 Operational Land Imager On-Orbit Geometric Calibration and Performance. Remote Sensing. 6 (11): 11127-11152.

[27]. Roy, D.P., Wulder, M.A., Loveland, T.R., Woodcock, C.E., Allen, R.G., Anderson, M.C., Helder, D., Irons, J.R., Johnson, D.M., Kennedy, R., Scambos, T.A., Schaaf, C.B., Schott, J.R., Sheng, Y., Vermote, E.F., Belward, A.S., Bindschadler, R., Cohen, W.B. and Zhu, Z. (2014). Landsat-8: Science and product vision for terrestrial global change research. Remote Sensing of Environment. 145: 154-172.

[28]. Ahmed, A. and Beiranvand Pour, A. (2014). Lithological mapping and hydrothermal alteration using Landsat 8 data: a case study in ariab mining district, red sea hills, Sudan. International Journal of Basic and Applied Sciences. 3 (3): 199-208.

[29]. Beiranvand Pour, A. and Hashim, M. (2015). Hydrothermal alteration mapping from Landsat-8 data,

Sar Cheshmeh copper mining district, south-eastern Islamic Republic of Iran. Journal of Taibah University for Science. 9 (2): 155-166.

[30]. Fotovat, H. and Solgi, A. (2014). Identification of altered tuff and supergene zone at Ferdows area, Iran prospecting for polymetal using Landsat- 8 and ASTER satellite images. Indian Journal of Fundamental and Applied Life Sciences. 4 (1): 53- 59.

[31]. Khalid, A.E.Z. and Eiman, A.M. (2014). Indicators of gold deposit near Khartoum, Sudan:Satellite gravity and Landsat- 8 OLI remote sensing data analysis. American Journal of Earth Sciences. 1 (2): 33-37.

[32]. Mwaniki, M.W., Moeller, M.S. and Schellmann, G. (2015). A comparison of Landsat 8 (OLI) and Landsat 7 (ETM+) in mapping geology and visualizing lineaments: A case study of central region Kenya, 36th International Symposium on Remote Sensing of Environment.Berlin. Germany.

[33]. Stoecklin, J. (1968). Structural history and tectonics of Iran; a review. Am Assoc Pet Geol Bull. 52 (7): 1229-1258.

[34]. Alavi, M. (1994). Tectonics of the Zagros orogenic belt of Iran: new data and interpretations. Tectonophysics. 229 (3-4): 211-238.

[35]. Hosseinjani Zadeh, M., Tangestani, M.H., Velasco Roldan, F. and Yusta, I. (2014). Mineral exploration and alteration zone mapping using mixture tuned matched filtering approach on ASTER data at the central part of Dehaj-Sarduiyeh copper belt, SE Iran. IEEE Journal of Selected Topics in Applied Earth Observations and Remote Sensing. 7 (1): 284-289.

[36]. Sorgan Parseh company. (2014). Final exploration report. Kerman. Iran.

[37]. Research Systems Inc. (2003). ENVI Tutorial, ENVI Software Package Version 4.0.

[38]. Gupta, R.P. (2003). Remote Sensing Geology. 2nd ed. Springer-Verlag Berlin Heidelberg. 671 P.

[39]. Mia, B. and Fujimitsu, Y. (2012). Mapping hydrothermal altered mineral deposits using Landsat 7 ETM^{+} image in and around Kuju volcano, Kyushu, Japan. Journal of Earth System Science. 121 (4): 1049-1057.

[40]. Mather, P.M. (2004). Computer Processing of Remotely Sensed Images: an introduction. 3rd ed. John Wiley & Sons. Chechester. England. 350 P.

[41]. Crosta, A.P. and Filho, C.R. (2003). Targeting key alteration minerals in epithermal deposits in Patagonia, Argentina, using ASTER imagery and principal component analysis. International Journal of Remote Sensing. 24 (21): 4233-4240.

نقشه‌برداری دگرسانی گرمابی با استفاده از داده لندست-۸ و کوئیک‌برد، مطالعه موردی: باب بیدوئیه، استان کرمان، ایران

حجت آرین‌مهر، مهدیه حسینجانی زاده*، مهدی هنرمند و فرزین ناصری

گروه اکولوژی، پژوهشگاه علوم و تکنولوژی پیشرفته و علوم محیطی، دانشگاه تحصیلات تکمیلی صنعتی و فناوری پیشرفته، کرمان، ایران

ارسال ۲۰۱۷/۳/۱۴، پذیرش ۲۰۱۷/۱۰/۱۶

* نویسنده مسئول مکاتبات:mh.hosseinjani@gmail.com

چکیده:

در این پژوهش تمرکز ما بر روی مجموعه داده لندست-۸ و کوئیک برای نقشه‌برداری دگرسانی گرمابی و گوسان در شناسایی کانه‌زایی مس پورفیری باب بیدوئیه است. این ناحیه در کمپلکس آتشفشانی- رسوبی ایران مرکزی جایی که ذخایر بزرگی مانند سرچشمه و چندین رخنمون متعدد مس وجود دارد، قرار گرفته است. با اجرای آنالیزهای مؤلفه اصلی و نسبت باندی بر روی مجموعه داده تصاویر لندست-۸ و کوئیک برد، زون‌های دگرسانی بارز شدند. نتایج پردازش تصویر با استفاده از مطالعات میدانی، تجزیه پراش اشعه ایکس (XRD)، مقاطع نازک میکروسکوپی و مطالعات طیف‌نمایی از نمونه‌های صحرایی و نیز نقشه‌های زمین‌شناختی ۱:۱۰۰۰۰۰ ساردوئیه و ۱:۵۰۰۰ باب‌بیدوئیه ارزیابی شدند. همچنین ویژگی‌های طیفی نمونه‌ها با بررسی بصری، نرم‌افزارهای PIMAView، SAMS و ViewSpecpro تجزیه و تحلیل شدند. ترکیب اندازه‌گیری‌های طیفی، آنالیز XRD و مطالعات سنگ‌شناسی نشان داد که مجموعه کانی‌ها نمونه بارزی از دگرسانی‌های فیلیک، فیلیک- سوپرژن، پروپیلیتیک، آرژلیک و گوسان هستند. نتایج به دست آمده از پردازش تصویر و آنالیز نمونه‌های صحرایی تأثیر اکسیدها و هیدروکسیدهای آهن را در سطح دگرسانی‌های فیلیک و آرژلیک نشان داد؛ بنابراین می‌توان نتیجه گرفت که نواحی گوسان بارز شده در کوئیک‌برد با نواحی دگرسانی فیلیک و آرژلیک مطابقت دارند.

کلمات کلیدی: نسبت باندی، دگرسانی گرمابی، لندست-۸، آنالیز مؤلفه اصلی، کوئیک‌برد.